THE JOURNAL OF BIOLOGICAL CHEMISTRY Vol. 280, No. 28, Issue of July 15, pp. 26457–26466, 2005

Printed in U.S.A.

Crystal Structure of Acetylcholine-binding Protein from *Bulinus truncatus* Reveals the Conserved Structural Scaffold and Sites of Variation in Nicotinic Acetylcholine Receptors*

Received for publication, December 22, 2004, and in revised form, April 25, 2005
Published, JBC Papers in Press, May 16, 2005, DOI 10.1074/jbc.M414476200

Patrick H. N. Celie‡§, Remco V. Klaassen¶§, Sarah E. van Rossum-Fikkert‡, René van Elk¶, Pim van Nierop¶, August B. Smit¶, and Titia K. Sixma‡‖

From the ‡Division of Molecular Carcinogenesis, Netherlands Cancer Institute, Plesmanlaan 121, 1066 CX Amsterdam, The Netherlands and ¶Department of Molecular and Cellular Neurobiology, Center for Neurogenomics and Cognitive Research, Faculty of Earth and Life Sciences, Vrije Universiteit, De Boelelaan 1085, 1081 HV Amsterdam, The Netherlands

The crystal structure of acetylcholine-binding protein (AChBP) from the mollusk *Lymnaea stagnalis* is the established model for the ligand binding domains of the ligand-gated ion channel family, which includes nicotinic acetylcholine, 5-hydroxytryptamine (5-HT_3), γ-aminobutyric acid (GABA), types A and C, and glycine receptors. Here we present the crystal structure of a remote homolog, AChBP from *Bulinus truncatus*, which reveals both the conserved structural scaffold and the sites of variation in this receptor family. These include rigid body movements of loops that are close to the transmembrane interface in the receptors and changes in the intermonomer contacts, which alter the pentamer stability drastically. Structural, pharmacological and mutational analysis of both AChBPs shows how 3 amino acid changes in the binding site contribute to a 5–10-fold difference in affinity for nicotinic ligands. Comparison of these structures will be valuable for improving structure-function studies of ligand-gated ion channel receptors, including signal transduction, homology modeling, and drug design.

Nicotinic acetylcholine receptors (nAChRs)[1] are members of the pentameric ligand-gated ion channel (LGIC) family that mediate and/or modulate synaptic signaling (1). nAChRs play important roles in memory and learning processes (2), and absence of functional receptors is associated with multiple diseases including schizophrenia, Alzheimer disease, drug addiction, and the autoimmune disease myasthenia gravis (3). nAChRs are also involved in nicotine addiction in tobacco smokers (4). Taken together, these receptors have prominent roles in disease of the nervous system and are now major targets in drug discovery programs.

nAChRs can be divided into muscular nicotinic receptors, which are found at the neuromuscular junction and have $(\alpha_1)_2\beta_1\delta\epsilon$ subunit stoichiometry, and neuronal nAChRs, which exist as homopentameric (*e.g.* α_7) or various heteropentameric (*e.g.* $\alpha_2\beta_4$) protein assemblies. To date 10 α- and 4β-nAChR subunits have been identified in vertebrates that generate a large diversity of nAChRs with distinct pharmacological and ligand binding characteristics. nAChRs are composed of an N-terminal extracellular ligand binding domain and a transmembrane region that forms the ion channel. Agonist binding stabilizes the open state of the channel and allows ions to pass through the pore (5). Ligand-binding sites are localized between two adjacent subunits, and residues from both subunits contribute to interaction with the ligand. An α subunit always contributes the principal side, and various subunits can contribute to the more variable complementary side of the interface.

It has been very difficult to obtain detailed structural information about these receptors. Electron microscopy analysis has resulted in a 4-Å resolution model of the transmembrane part, which provided insight into the structural and functional aspects of channel opening (6). Structural information about the ligand binding domains and the subunit interfaces has expanded upon discovery and crystallization of acetylcholine-binding protein from the snail *Lymnaea stagnalis* (Ls-AChBP) (7, 8), a soluble homologue of the nAChR ligand binding domain. This crystal structure has been embraced as an excellent model for analyzing the ligand binding domains of nAChR (9–12) GABA (13–14), glycine (15), and 5-HT_3 (16) receptors. The application of AChBP as a LGIC model is further supported by recent experiments showing that AChBP can be functionally coupled to the transmembrane region of a 5-HT_3 receptor (17). The recent crystal structures of Ls-AChBP in complex with nicotine and carbamylcholine have elucidated the molecular contacts between ligand and protein and are in excellent agreement with biochemical data obtained from nAChR binding studies (18). These structures also emphasize the importance of obtaining different high resolution AChBP structures for improving modeling studies as they reveal movements within the protein that are difficult to infer from homology

* This work was supported by STW (Stichting Technische Wetenschappen), Project BBC6035, by the Netherlands Organization for Research in Chemistry (NWO-CW), Project 98016, and by EU-SPINE. The costs of publication of this article were defrayed in part by the payment of page charges. This article must therefore be hereby marked "*advertisement*" in accordance with 18 U.S.C. Section 1734 solely to indicate this fact.

The atomic coordinates and structure factors (code 2BJ0) have been deposited in the Protein Data Bank, Research Collaboratory for Structural Bioinformatics, Rutgers University, New Brunswick, NJ (http://www.rcsb.org/).

The nucleotide sequence(s) reported in this paper has been submitted to the GenBank™/EBI Data Bank with accession number(s) CAC69294 and CAC69295.

§ These authors contributed equally to this work.

‖ To whom correspondence should be addressed. Tel.: 31-20-5121959; Fax: 31-205121954; E-mail: t.sixma@nki.nl.

[1] The abbreviations used are: nAChR, nicotinic acetylcholine receptor; Ls-AChBP, *L. stagnalis* acetylcholine-binding protein; Ac-AChBP, *A. californica* acetylcholine-binding protein; Bt-AChBP, *B. truncatus* AChBP acetylcholine-binding protein; LGIC, ligand-gated ion channel; 5-HT_3, 5-hydroxytryptamine; CAPS, 3-(cyclohexylamino)-1-propanesulfonic acid; ITC, isothermal titration calorimetry; r.m.s., root mean square; GABA, γ-aminobutyric acid.

models. The discovery of AChBP has led to the identification and biochemical characterization of AChBP from the snail *Aplysia californica* (Ac-AChBP) that shows distinct ligand binding properties compared with that of Ls-AChBP (19).

Here we present the pharmacology and x-ray structure of *Bulinus truncatus* AChBP (Bt-AChBP) and use it to analyze differences in sequence and the concomitant diversity in ligand binding characteristics. We noticed earlier that sequence diversity between subunits is most notable at the subunit interfaces, which lack conserved sites of interaction apart from the ligand-binding site (8). Here we show that these differences in subunit interface have a significant effect on the stability of the AChBP pentamers. Using isothermal titration calorimetry (ITC), we have analyzed ligand binding to Bt-AChBP and Ls-AChBP/Bt-AChBP substitution mutants to identify the residues that are responsible for differences in ligand binding affinity. Because the variations in interface contacts and ligand binding are similar to those observed between mammalian receptor subtypes, they provide an essential analysis to unravel the conserved scaffold of the LGIC ligand binding domains.

EXPERIMENTAL PROCEDURES

Cloning of B. truncatus AChBP—Live *B. truncatus* specimens were obtained from the river Nile delta (Egypt) and subsequently cultured in the laboratory under standard (*Lymnaea*) freshwater conditions. Poly(A) RNA was isolated from the central nervous system. cDNA was generated by reverse transcription using the primer RoRi-(dT_{17}) (5′-ATCGATGGTCGACGCATGCGGATCCAAAGCTTGAATTCGAGC-TCT(dT_{17})-3′). For the identification of Bt-AChBP homologues, a nested PCR strategy was adopted using degenerate oligonucleotides designed to match conserved regions of Ls-AChBP and the nAChRa7 as well as to unique AChBP sequence features. Two nested primers were designed, BABP1 (5′-GA(A/G)AG(C/T)GGNGCNACNTG(T/C)(C/A)G-NAT(A/T/C)AA-3′) and BABP2 (5′-CGGAATTCTG(T/C)(C/A)GNAT(A/T/C)AA(A/G)GTNGGNAG(C/T)TGG-3′). A first PCR was performed using 50 pmol of BABP1 primer in combination with 50 pmol of the first adaptor primer Ro (5′-ATCGATGGTCGACGCATGCGGATCC-3′) on the RoRi-generated cDNA template in a volume of 100 μl for 40 cycles (94 °C, 30 s; 63 °C, 45 s; 72 °C, 2 min). To increase specificity, a second round of nested amplification was carried out on 1% of the previous PCR reaction mixture using 50 pmol of BABP2 in combination with 50 pmol of nested adaptor primers Ri (5′-GGATCCAAAGCTTGAATTC-GAGCTCT-3′) under identical conditions as described above. PCR products from the reaction were separated on agarose gel, and DNA products of appropriate size were isolated, subcloned in pBluescript KS(+) (Stratagene), and sequenced. The full-length Bt-AChBP cDNA was obtained by 5′ rapid amplification of cDNA ends on cDNA templates derived from *Bulinus* central nervous system using a cloning and sequence strategy as described earlier (20). Possible DNA sequence errors introduced by PCR amplification were eliminated by sequence comparison of three independently generated PCRs products.

In Situ Hybridization—Localization of Bt-AChBP mRNA was studied in sections of the central nervous system with *in situ* hybridization using digoxigenin-UTP-labeled cRNA probes. Tissue was fixed in 1% paraformaldehyde and 1% acetic acid for 36 h and embedded in paraffin. Sections of 5-μm thickness were adhered to SuperFrost-Plus slides (21). After dewaxing, sections were fixed with 2% paraformaldehyde in phosphate-buffered saline at room temperature for 4 min and 1% hydroxylammonium chloride in phosphate-buffered saline for 15 min. Next, the slides were dehydrated in alcohol and air-dried. Digoxigenin-labeled cRNA probes (sense and antisense) were made on 40 ng of a PCR fragment corresponding to positions 230–511 of the Bt-AChBP open reading frame that included T3 and T7 RNA polymerase promoters. *In vitro* transcription was performed using either T3 or T7 RNA polymerase containing 1 mM GTP/ATP/CTP, 0.65 mM UTP, and 0.35 mM digoxigenin-11-UTP. Reactions were stopped after 2 h of incubation, treated with 20 units of DNase I (Roche Applied Science) at 37 °C for 10 min, hydrolyzed with 0.2 M NaOH on ice for 30 min, neutralized with Tris-HCl, and ethanol-precipitated. About 10% of the cRNA formed was added per slide. Hybridization was done in 60% formamide at 50 °C for 16 h, washed in 2× SSC (1× SSC = 0.15 M NaCl and 0.015 M sodium citrate), 50% formamide for 15 min 55 °C, 100 ng/ml RNase A for 25 min, 2× SSC, 50% formamide at 55 °C for 3 × 15 min, and 2× SSC at room temperature for 2 × 5 min. Next, the digoxigenin was visualized using an alkaline phosphatase-labeled antibody directed to digoxigenin.

Protein Preparation—The Bt-AChBP gene including its signal sequence was expressed in baculovirus using the pFastbac I vector according to Invitrogen protocols. Secreted AChBP was purified 72 h after infection of SF9 cells as described for Ls-AChBP (18). The yield was 5 mg/liter, giving a single molecular species with an M_r of ~250,000 in gel filtration and multi-angle laser light scattering experiments using a Wyatt Technology miniDAWN on-line with a Superdex 200 gel filtration column. SDS-PAGE and mass spectrometry analysis revealed the presence of a single subunit species (M_r 23,758), indicating that purified Bt-AChBP exists as a stable decamer. The calculated mass of the monomer is 22,938, suggesting that glycosyl groups of M_r ~ 820 are attached to the potential glycosylation sites Asn-21 and Asn-26.

Crystallization—Crystals of Bt-AChBP were grown at room temperature using the hanging drop method. The best crystals were obtained at relatively low protein concentrations (0.2–0.5 mg/ml). Orthorhombic crystals ($C222_1$) of AChBP were grown in a solution of 2.0 M ammonium sulfate, 200 mM lithium sulfate, and 0.1 M CAPS, pH 10.5. Cell constants are: a = 76.95 Å, b = 219.02 Å, c = 166.97 Å, and 1 pentamer per asymmetric unit.

Structure Solution and Refinement—We collected data at ID14 EH4 at the European Synchrotron Radiation Facility (Grenoble, France). MOSFLM (22) was used for indexing of data and designing the optimal data collection strategy. Data were processed and scaled using DENZO and SCALEPACK (23). Programs in the CCP4 suite were used to build and refine the model. An initial model was built with the AMORE molecular replacement program (22) using the HEPES-bound Ls-AChBP pentamer (18) as the search model. Automated model building was performed using ARP/wARP (24). The structure was rebuilt in O (25) and refined with REFMAC, including TLS refinement (26). The final model has been refined without any non-crystallographic symmetry restraints. CAPS buffer molecules were built and refined at the final stages of refinement. A CAPS buffer molecule could be built within 4 ligand-binding sites in the asymmetric unit (56 atoms in total). In one of these sites the CAPS molecule was estimated to have ~75% occupancy, whereas density in the 5th site indicated the presence of solute molecules rather than a CAPS molecule. Water molecules were found using the ARP/wARP program (24) in combination with REFMAC cycles.

Structure Analysis—Optimized multiple superposition was obtained with LSQMAN (27). Structure analysis was performed with CCP4 programs (22) and central nervous system (28). Interface analysis was performed with CCP4 programs and the EBI web server. The figures were made with ESPript (29) and PyMol (W. L. DeLano, San Carlos, CA).

Circular Dichroism—CD spectra were recorded in the far UV range (195–260 nm) in quartz cells with a 1-mm path length and in the near UV range (250–320 nm) in 5-mm-path length cells on a Jasco (Tokyo, Japan) J-810 CD spectropolarimeter. Proteins were dialyzed against 20 mM sodium phosphate buffer, pH 8.0, and diluted to 0.4 and 2 mg/ml for CD measurements in the far UV and near UV region, respectively. Thermal stability was monitored by collecting spectra at different temperatures between 25 and 90 °C. Solutions were equilibrated for 5 min at selective temperatures before spectra were recorded.

Bungarotoxin Binding—Biotinylated bungarotoxin (16 μM) was incubated with AChBP (3 μM) in 50 μl of buffer containing 100 mM NaCl and 20 mM Tris, pH 8.0, for 1 h at room temperature. 25 μl of streptavidin beads were added to the solution to precipitate α-bungarotoxin-(AChBP). Supernatant was removed, and beads were washed 3 times with 100 mM NaCl and 20 mM Tris, pH 8.0. Proteins were eluted from the beads by boiling in sample buffer and subsequently loaded on SDS-PAGE. Protein bands were visualized by Coomassie staining.

Isothermal Titration Calorimetry—ITC experiments were performed with the VP-ITC MicroCalorimeter (MicroCal, Inc.) in 100 mM NaCl, 25 mM phosphate buffer, pH 8.0, as described previously (18). Data points were fitted to a model describing a single type of binding site using software supplied by the ITC manufacturer.

RESULTS

Identification and Cloning of B. truncatus AChBP—We analyzed *B. truncatus* central nervous system-derived cDNA templates for the presence of AChBP homologs using a PCR strategy and degenerate oligonucleotides designed to target potentially sequence-conserved regions in Ls-AChBP. The obtained sequences were made full-length by 5′ and 3′ rapid amplification of cDNA ends. Two AChBP homologs, Bt-AChBP

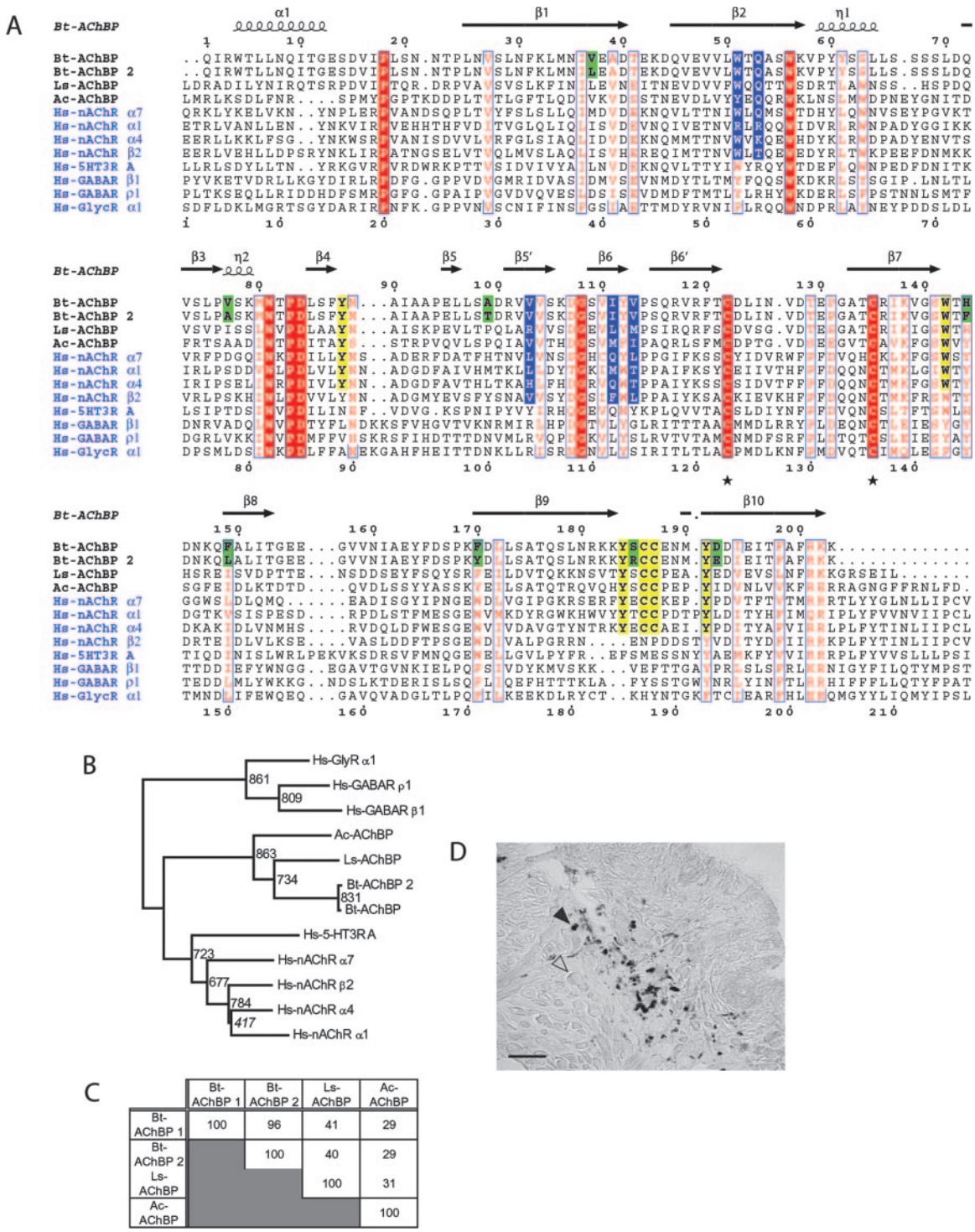

FIG. 1. **Comparison of Bt-AChBP to other AChBPs and LGIC receptors.** *A*, ClustalX protein sequence alignment of Bt-AChBP, AChBP homologs and subunits of the Cys-loop family of LGICs. Alignment is shown from the first residue of Ls-AChBP to the last of Ac-AChBP. Represented on *top* are the secondary structure elements of Bt-AChBP (α, α-helix; β, β-strand; η, 3_{10}-helix). Indicated are residues of the principal (*yellow*) and complementary (*blue*) components of the nicotinic ligand-binding site as well as positions different in Bt-AChBP types 1 and 2 (*green*). Identical (*red*) and conserved (*red letters*) residues are marked. *Stars* indicate beginning and end of the conserved Cys-loop. *B*, phylogenetic analysis of AChBP homologs and human Cys-loop family subunits. An unrooted tree was calculated on aligned protein sequences (as shown in *panel A*) by the maximum likelihood method using Phylip (49). Bootstrap values of 1000 scrambled data sets are indicated at branches; sub-threshold bootstrap value displayed in *italic*. *C*, identity table of AChBP homologs representing the percentages of identical residues on corresponding positions. *Hs*, *Homo sapiens*; *Bt*, *B. truncatus*; *Ls*, *L. stagnalis*; *Ac*, *A. californica*. *D*, *in situ* hybridization on *Bulinus* central nervous system showing the presence of Bt-AChBP transcripts in glial cells (*solid arrowhead*) and not in neurons (*open arrowhead*). *Scale bar*, 20 mm. No signal was observed for sense probe hybridizations.

and Bt-AChBP-2, were identified with 96% sequence identity. Bt-AChBP is expressed in glial cells of the central nervous system of the animal (Fig. 1*D*), similar to the expression of Ls-AChBP (7). In Fig. 1*A* a sequence comparison of the AChBPs and members of the Cys-loop family show that Bt-AChBP shares 41% sequence identity with Ls-AChBP, 29% with the recently characterized Ac-AChBP (19) (Fig. 1*C*), and 13–25% with LGIC subunits.

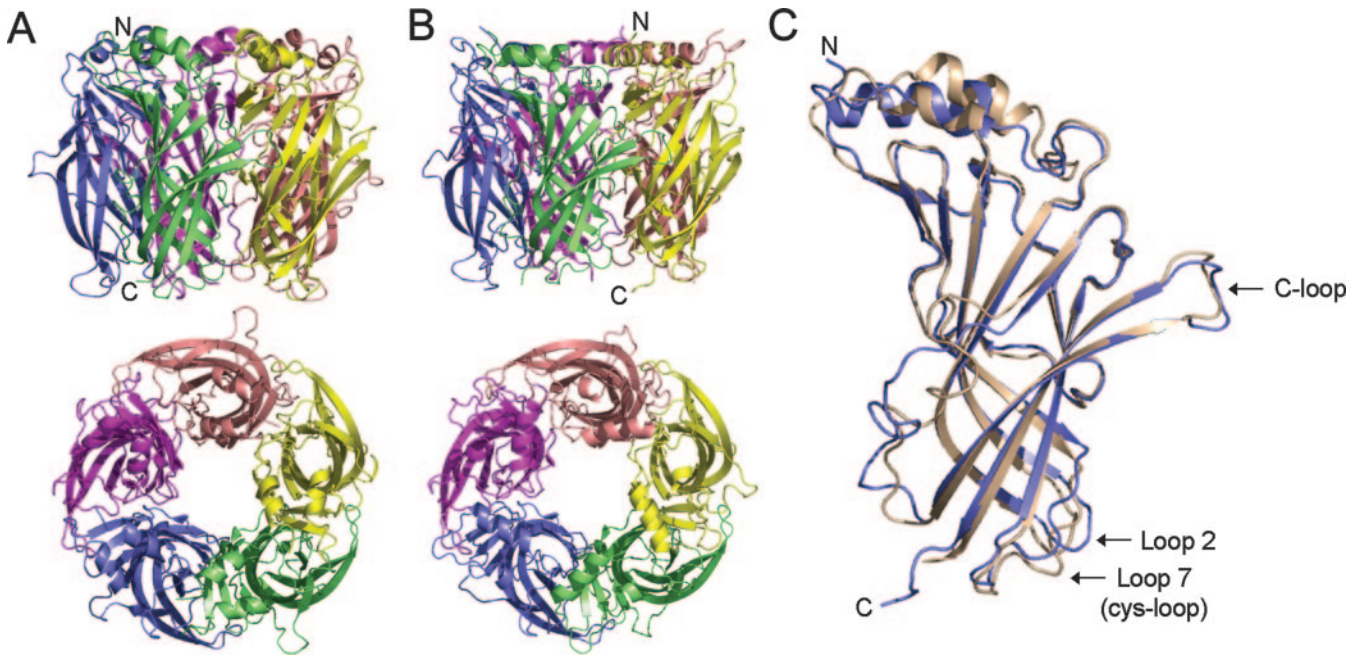

FIG. 2. **The crystal structure of Bt-AChBP.** The pentamer structure in the side and top view of Bt-AChBP (*A*) compared with Ls-AChBP (*B*) in a schematic representation with each monomer in a different color. In the side view the N-terminal region (indicated by *N*) is at the *top*, and the nAChR transmembrane domain would be at the *bottom* near the C terminus (indicated by *C*). *C*, side view of a superposition of one monomer of Bt-AChBP (*wheat*) on Ls-AChBP (*blue*).

The *Bulinus* protein and the other AChBPs contain a functionally conserved nAChR ligand-binding site. All residues on the principal side (loop A, Tyr-88; loop B, Trp-142; loop C, Tyr-*X*-Cys-Cys-*X*-Tyr motif) are present, and the residues on the complementary side are conserved (loop D, Trp-51 and Gln-53) or fall within the sequence variation that is observed in nicotinic receptors (loop E). Residues of the subunit interface, however, show very little conservation in Bt-AChBP and the other AChBPs. This variability is also found between members of the LGICs (8), suggesting that the conserved ligand-binding site and the monomer interface have evolved as discrete parts during evolution.

We produced Bt-AChBP and Bt-AChBP-2 in the yeast *Pichia pastoris* and in a baculovirus expression system in Sf9 insect cells. Although the two Bt-AChBPs share 96% sequence identity with conservative substitutions, Bt-AChBP-2 did not express well in a heterologous system, and we decided to focus on the characterization of Bt-AChBP. In solution, the purified protein behaves as a decamer, as shown by gel filtration and multi-angle laser light scattering (data not shown), in contrast to the *Lymnaea* protein, which behaves as a pentamer. However, the decamer observed in solution for the *Bulinus* protein is also seen for the *Lymnaea* protein in the crystallographic packing in most crystal forms.

Crystal Structure of Bt-AChBP—The Bt-AChBP crystal structure was determined at 2.0 Å by molecular replacement with the Ls-AChBP structure as a search model (Fig. 2). In contrast to all Ls-AChBP structures, the crystallographic data were excellent and did not require non-crystallographic symmetry (Table I). Refinement resulted in an *R*-factor of 20.9% and free *R*-factor of 24.9%, in which residues Gln-1–Lys-203 from each subunit could be built into the electron density. There are two potential *N*-glycosylation sites at Asn-21 and Asn-26, but weak sugar density indicates that only Asn-26 is glycosylated. The r. m. s. deviation between subunits is between 0.25 and 0.45 Å on 196 Cαs, excluding the major varying region (residues 154–161) in the F-loop.

Bt-AChBP was crystallized in the presence of CAPS buffer, pH 10.5, and a CAPS molecule could be built with confidence into the electron density in four of five binding sites. Three sites are fully occupied by CAPS, whereas the fourth site shows a lower occupancy (75%). The electron density at the fifth site indicates a low occupancy of CAPS and the presence of solute molecules. Interestingly, double conformations of Tyr-88 were observed in the two binding sites with the lower occupancy of CAPS, illustrating the movement of the tyrosine side chain upon ligand binding. This ligand-dependent change is similar to that observed for Tyr-89 in Ls-AChBP (18). After superposition of Bt-AChBP and Ls-AChBP with nicotine bound, CAPS and nicotine closely superimpose with positive nitrogen positions agreeing within 1.1 Å. No CAPS binding could be identified in bungarotoxin competition studies and ITC, indicating that the binding affinity is very weak. Contacts of the CAPS molecule are given in Fig. 3, showing hydrogen bond interac-

TABLE I
Crystallographic parameters

Space group	$C222_1$
Unit cell parameters	
a	77.0
b	219.0
c	167.0
Resolution (Å)	50–2.0
Redundancy	5.1 (3.4)[a]
R_{merge} (%)[b]	12.9 (77.9)
$I/sigI$	12 (1.7)
Mosaicity (°)	0.74
Completeness (%)	98 (89)
Refinement	
Resolution (Å)	12–2.0
Reflections	88,439
Atoms	8,566
R factor (%)[c]	20.9
R_{free} (%)[d]	24.9
r.m.s. bonds (%)	0.013
r.m.s. angle (°)	1.523

[a] Values in parentheses correspond to the highest resolution data shell (2.07–2.0 Å).
[b] $R_{merge} = \Sigma|I - \langle I\rangle|/\Sigma\langle I\rangle$.
[c] *R*-factor = $\Sigma||F_{obs}| - |F_{calc}||/\Sigma|F_{obs}|$.
[d] R_{free} = *R*-factor for 5% of reflections that were not used in refinement.

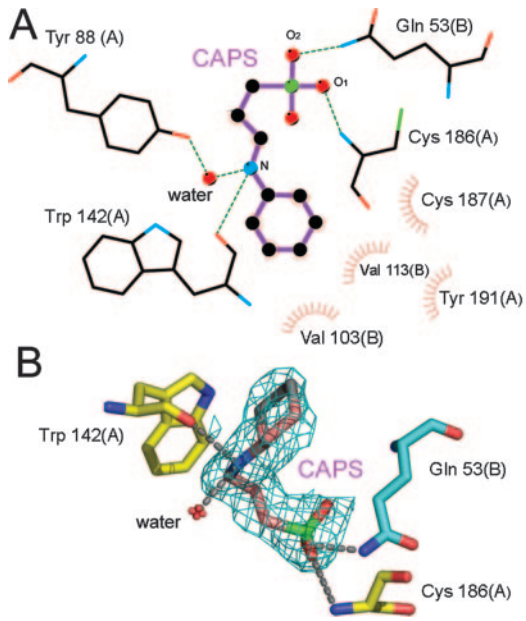

FIG. 3. **CAPS binding to Bt-AChBP.** A CAPS buffer molecule is bound in the ligand-binding site of Bt-AChBP. *A*, LIGPLOT representation (50) showing CAPS contacts with subunit A (principal side) and subunit B (complementary side). *B*, electron density of CAPS in *ball-and-stick model* showing hydrogen bonds to the protein.

tions with the carbonyl oxygen of Trp-142 to the positive charge in the buffer, as was observed for other agonists. Two additional hydrogen bonds are seen to the sulfate portion of the molecule.

Structural Comparison to Ls-AChBP—The structure of Bt-AChBP is remarkably similar to that of Ls-AChBP despite the low sequence conservation. All secondary structure elements are conserved, and most of these are of equal length (Fig. 4*A*) in the two snail AChBPs. In automated superposition of the individual domains using LSQMAN, a core of 170–180 Cα atoms superimposes, with an r.m.s. density of 1.2 Å against each of the three high resolution structures of Ls-AChBP (18).

Comparison of the entire AChBP pentamers, based on a superposition of the Cα atoms of the core residues of each subunit, shows that differences between both AChBPs are limited to structural variation within each subunit itself rather than a change in the relative orientation of the subunits. The most pronounced differences are at the "top" of the molecule, furthest from the membrane interface in nAChRs (Fig. 2*B*). There the N-terminal helix is differently oriented, and the β2-β3 region is reorganized and includes a longer 3^{10} helix. The decamer of the *Bulinus* protein is formed by a crystallographic 2-fold axis, stacking the pentamers with their N termini to each other. Residues that are responsible for decamer formation are not conserved in Ls-AChBP. These include 10 salt bridges between residues Arg-3 and Glu-13 in all Bt-AChBP subunits. The loop 9 (or F-loop region, residues 155–167) that is disordered in most of the Ls-AChBP subunits also has a different structure in the *Bulinus* protein.

The most striking difference between Ls- and Bt-AChBP is the conformation of a series of critical loops on the side of the pentamer that would be close to the transmembrane region in the LGICs, loops 2 (residues 41–44) and 7 (Cys-loop, residues 122–135), and the C terminus (loop 11, residues 200–203) (Fig. 2*B*). All these loops are oriented differently with respect to the AChBP core between the two species due to rigid body shifts. These rigid body shifts are intriguing, and several explanations for this shift in orientation can be given. They could be an intrinsic feature of the Bt-AChBP structure, or alternatively, they could be due to the high pH of the crystallization buffer or the result from CAPS binding.

Pentamer Interface and Stability—In our initial analysis of the Ls-AChBP structure we noticed that the interface between monomers was poorly conserved between different LGIC subfamilies and that most of the conserved residues contribute to the hydrophobic core of the monomer (8). The availability of a second crystal structure provides the opportunity to analyze what the effect is of such a variable interface. This is essential because these interfaces harbor the conserved ligand-binding site. In the pentamer structure each monomer contributes to two separate interfaces. Thus, the A subunit contributes its so-called "principal side" to the AB interface and its "complementary side" to the EA interface. *Below* the alignment of Fig. 4*A*, an analysis of the monomer A residues in the AB (indicated by *B*) and the EA interface (indicated by *E*) are given for the two molluscan AChBP crystal structures. From this comparison it is clear that, although the same loops are involved in the protein-protein interface, the actual contacts are completely different. The only residues that make similar contacts are found in the binding site. The mapping of interface residues onto the surface of the monomer shows that indeed the interfaces are very different (Fig. 4, *B–E*). However, the overall characteristics of these interfaces are highly similar in terms of size, hydrophobicity, and accessible surface area.

To obtain a better understanding of the stability of the interface, we used CD to compare the thermal stability of the molluscan AChBPs. As expected, spectra recorded for Bt-AChBP and Ls-AChBP at the far UV region show the characteristics of a structure that is largely composed of β-sheets (Fig. 5, *A* and *B*). They are similar to the spectrum obtained for the monomeric ligand binding domain of the muscle α-subunit from mouse (30), reconfirming that the structures are very similar. The spectra measured in the near UV region are indicative of proteins with a well defined tertiary structure (Fig. 5, *C* and *D*). The signals are attributable to phenylalanine, tyrosine, and tryptophan residues as well as to disulfide bonds. The profiles, however, are different, presumably due to differences in the local environment of aromatic residues that influence the absorption of these residues.

From a series of spectra measured at increasing temperatures (Fig. 5) we observed a significant difference in stability. Ls-AChBP only starts to melt at 65 °C, whereas Bt-AChBP has its transition between 50 and 55 °C. We could see the same shift in both the far and near UV region. Because we do not seem to lose the β-sheet structure completely, it is likely that the individual monomers do not unfold entirely and that the transition that we observe primarily reflects the loss of the multimeric structure. Thermal denaturation was irreversible for both AChBPs (data not shown), indicating that refolding of the multimeric state was not possible. The high stability of the secondary structure upon heating has also been observed for the ligand binding domain of the muscle α-subunit from mouse (30) and for other proteins containing a substantial number of β-strands (31).

Although Ls-AChBP is considerably more stable, it is difficult to attribute this to any specific structural parameter. In the Ls-AChBP structure each interface has on average one extra hydrogen bond and two additional salt bridges. However, salt bridges are difficult to evaluate in the Bt-AChBP structure due to the extreme pH (10.5) of the crystals. It is possible that *e.g.* the pair of Asp-84 and Arg-101 on the principal and complementary side, respectively, would form an additional salt bridge at lower pH. The precise number of hydrogen bonds also changes slightly between the different ligand-bound struc-

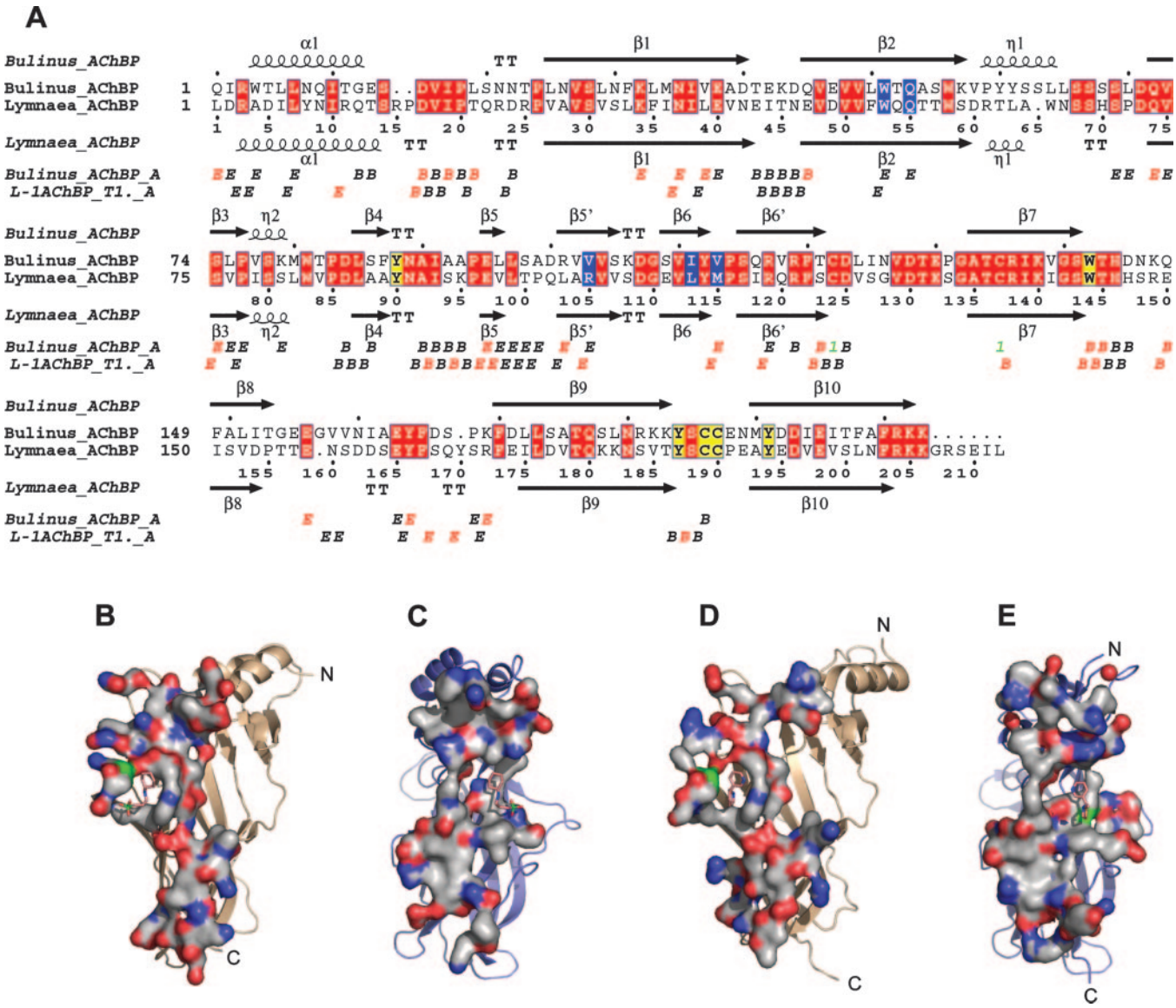

FIG. 4. **The subunit interface.** *A*, sequence alignment showing Bt- and Ls-AChBP conservation, secondary structures, and residues involved in subunit interfaces. These are indicated *below* the alignment, with B if located on the principal side of the interface and with E if located at complementary side of the interface, colored in *red* if within hydrogen-bonding distance or in *black* if within van der Waals contact to the other subunit; residues forming the principal binding site (*yellow boxes*) and the complementary binding site (*blue boxes*) are indicated. The figure is generated with ESPript (29). *B–E*, opening up of subunit interface. Residues that are part of the interface are shown in a surface representation and are colored by atom type (*red*, oxygen; *blue*, nitrogen; *white*, carbon; *green*, sulfur), with the ligand shown in *ball-and-stick* of the Bt-AChBP principal side (*B*) and Bt-AChBP complementary side (*C*). *D*, Ls-AChBP principal side; *E*, Ls-AChBP complementary side.

tures, dependent on the position of residues that touch the ligand. Altogether, the large differences in interface contact make it difficult to assess the precise region that contributes to the variation in stability.

Ligand Binding—Because the ligand-binding site is part of the monomer interface, we next assessed differences in ligand binding properties of Bt-AChBP and Ls-AChBP. We first determined the binding curve of I^{125}-labeled α-bungarotoxin to Bt-AChBP. In contrast to Ls-AChBP, Bt-AChBP does not bind significantly to α-bungarotoxin (data not shown). This is confirmed by the absence of Bt-AChBP-bungarotoxin complex when biotinylated bungarotoxin was used in a pull-down assay (Fig. 6*A*). Bt-AChBP contains a lysine at position 183, similar to the human α_2, α_3, and α_4 subunits that do not bind to the toxin. NMR and mutagenesis studies have shown that nAChRs that bind to α-bungarotoxin have a tyrosine or phenylalanine at this position (32–34) and that replacement of this tyrosine by lysine completely prevents binding of α-bungarotoxin (34, 35).

To obtain detailed insight in the ligand binding characteristics of Bt-AChBP, we analyzed the binding to several ligands using ITC. Bt-AChBP shows up to 10-fold higher affinity for nAChR agonists when compared with Ls-AChBP (Table II). The increase in affinity can be attributed to a more favorable enthalpy change (ΔH) even though the change in entropy (ΔS) has a more unfavorable contribution to the affinity. Because the ΔH value represents the strength of molecular interactions, Bt-AChBP apparently forms more and/or tighter interactions with these agonists.

The nAChR antagonist *d*-tubocurarine is bound with very high affinity to Ls-AChBP (Table II, Fig. 6*B*). In contrast to agonist binding, however, ΔS then has a favorable effect on binding, whereas the contribution of ΔH is ~2-fold reduced. Binding of *d*-tubocurarine to Bt-AChBP also appears to be largely determined by ΔS, but thermodynamic parameters cannot be measured accurately because of the very small heat signals that are recorded (Fig. 6*C*).

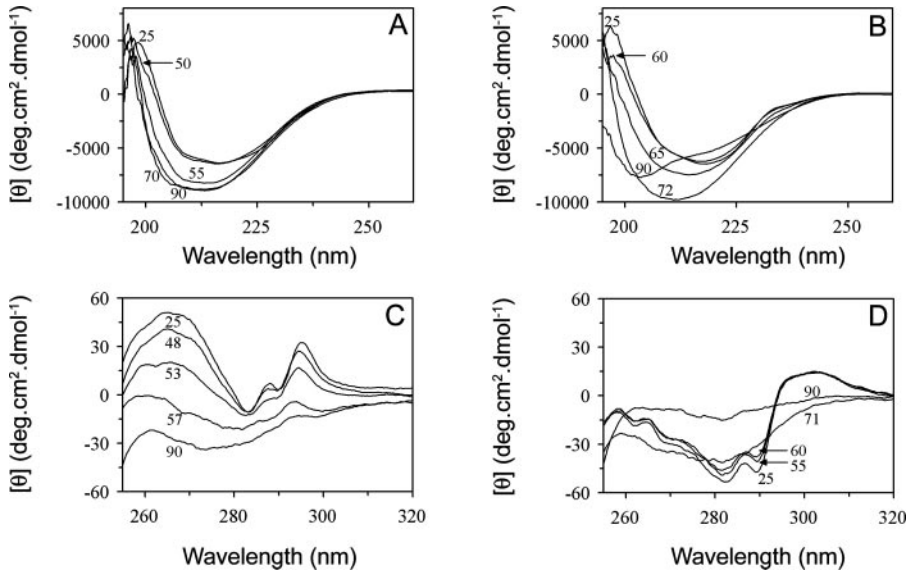

FIG. 5. **Stability of AChBPs upon heat denaturation.** CD spectra were recorded at increasing temperatures (25–90 °C) in the far UV region (195–260 nm) for Bt-AChBP (*A*) and Ls-AChBP (*B*). CD spectra in the near UV region were recorded between 250–320 nm for Bt-AChBP (*C*) and Ls-AChBP (*D*). All graphs contain a selection of the spectra that were recorded at various temperatures. Temperatures (in °C) are indicated for each spectrum that is displayed.

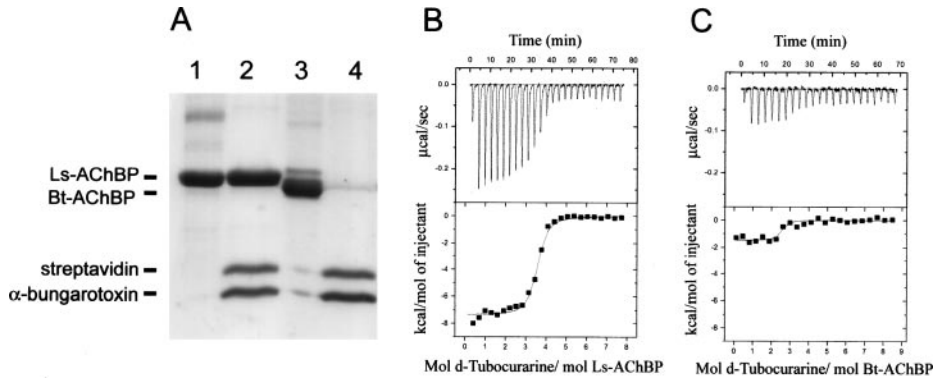

FIG. 6. **Ligand binding to Bt-AChBP.** *A*, α-bungarotoxin pull-down experiment on purified Ls-AChBP and Bt-AChBP as described under "Experimental Procedures." Samples of purified Ls-AChBP and Bt-AChBP (*lanes 1* and *3*, respectively) were incubated with biotin-labeled α-bungarotoxin and streptavidin beads. Proteins that are bound to the beads after incubation with Ls-AChBP and Bt-AChBP (*lanes 2* and *4*, respectively) were eluted from the beads by boiling in sample buffer and loaded on SDS-PAGE. Protein bands were visualized by Coomassie Blue staining. ITC binding curves of *d*-tubocurarine binding to Ls-AChBP (*B*) and Bt-AChBP (*C*) are shown. The *top panels* show the heat response upon each injection of *d*-tubocurarine into AChBP solution. Data points obtained from integration of the heat signals are plotted in the *bottom panels* and fitted to a model describing a single type of binding site.

Modulation of Binding by Variation of the Complementary Binding Site—Because the ligand affinities for Bt-AChBP and Ls-AChBP show a 5–10-fold difference, this leaves the possibilities that these differences are attributable to the earlier measured dissimilarities in interfaces and stability or that they are directly caused by a discrepancy in residues within the ligand-binding site itself. Because only three ligand binding residues are different between the two AChBP species, we tested whether mutation of these residues in the *Lymnaea* protein would generate an increase in affinity similar to that observed for Bt-AChBP. Therefore, we mutated the side chains of Arg-104, Leu-112, and Met-114 in the complementary binding site of Ls-AChBP into the corresponding residues in Bt-AChBP (Val-103, Ile-111, and Val-113, respectively) (Fig. 7*B*) and studied the binding properties using ITC (Table II).

The Ls-AChBP-M114V and Ls-AChBP-R104V substitution variants display a selective increase in affinity for nicotine (Table II), whereas the affinity of the Ls-AChBP-L112I mutant is lower than either Ls-AChBP or Bt-AChBP. The effect of the mutants on nicotine binding can be explained by analysis of the AChBP structures. The negative effect of the L112I substitution seems to be caused by loss of hydrophobic contact, because Ile-111 in the Bt-AChBP structure is positioned away from the ligand (Fig. 7*B*), whereas the leucine side chain makes good contact with both nicotine and acetylcholine (18). The opposite effect is true for the Ls-AChBP-R104V mutation; the extended side chain of Arg-104 does not contact nicotine, but the branched side chain of the valine provides a beneficial hydrophobic contact to the CAPS binding in Bt-AChBP and would also do so for nicotine. The positive effect of the M114V mutation can be explained by nicotine forcing the methionine side chain Cϵ into an unusual rotamer position to avoid a direct clash with nicotine (18). Thus, the substitution of a smaller side chain is beneficial for nicotine binding. The critical role of residue 114 in ligand binding affinity is further stressed by the fact that mutation of M114V causes a 5-fold increase in affinity for *d*-tubocurarine (Table II), whereas M114Y and M114T substitutions reduce binding 6- and 11-fold, respectively (36).

The effects of acetylcholine binding on mutations at the 112 and 114 position are in line with the structural analysis above, but the double mutant result cannot be simply explained. In addition, the strongly detrimental effect of the R104V mutant and the resulting effect on the triple mutant cannot be explained from the structural analysis. One possibility may be that loss of a salt bridge between Arg-104 and Glu-147 (Gln-148 in Bt-AChBP) in the R104V mutant is unfavorable for acetylcholine binding. Alternatively, additional residues/regions (*e.g.* F-loop) outside the binding site could have ligand-specific contributions that cannot be easily predicted from our structures.

TABLE II
Thermodynamic parameters of AChBP-ligand interaction

AChBP-ligand interactions were studied using isothermal titration calorimetry. Data represent the mean (±S.D.) of at least two separate experiments. Dissociation constants (K_d) and thermodynamic parameters ΔH (enthalpy change) and ΔS (entropy change) were determined by titration of ligands into AChBP in 100 mM NaCl, 25 mM phosphate buffer, pH 8.0, at 22 °C. ΔC_p (heat capacity) was calculated from the slope of linear fits of ΔH *versus* temperature (T) as shown in Fig. 7*C*.

Protein	Ligand	K_d	ΔH	$-T\Delta S$	ΔC_p
		nM	*kcal mol*$^{-1}$	*kcal mol*$^{-1}$	*cal mol*$^{-1}$ *K*$^{-1}$
Ls-AChBP	Nicotine[a]	45 ± 2	−14.5 ± 0.2	4.5 ± 0.1	−207 ± 15
Bt-AChBP	Nicotine	8 ± 4	−17.5 ± 0.3	6.5 ± 0.6	−383 ± 10
Ls-R104V	Nicotine	22 ± 1	−14.1 ± 0.1	3.3 ± 0.1	−270 ± 1
Ls-L112I	Nicotine	253 ± 28	−11.4 ± 0.2	2.5 ± 0.1	−146 ± 9
Ls-M114V	Nicotine	18 ± 4	−13.9 ± 1.6	4.3 ± 0.2	−225 ± 2
Ls-L112I/M114V	Nicotine	59 ± 9	−12.7 ± 0.1	3.0 ± 0.1	ND[b]
Ls-R104V/L112I/M114V	Nicotine	12 ± 1	−15.0 ± 0.3	4.1 ± 0.3	−345 ± 19
Ls-AChBP	Acetylcholine[a]	823 ± 40	−12.5 ± 0.1	4.2 ± 0.3	−126 ± 13
Bt-AChBP	Acetylcholine	153 ± 23	−16.3 ± 0.4	7.0 ± 0.5	−327 ± 3
Ls-R104V	Acetylcholine	>10,000			ND
Ls-L112I	Acetylcholine	2870 ± 396	−12.3 ± 0.6	4.8 ± 0.7	ND
Ls-M114V	Acetylcholine	1710 ± 226	−16.3 ± 0.8	8.6 ± 1.5	ND
Ls-L112I/M114V	Acetylcholine	1120 ± 47	−9.5 ± 0.8	1.5 ± 0.9	ND
Ls-R104V/L112I/M114V	Acetylcholine	>10,000			ND
Ls-AChBP	Carbamylcholine[a]	7575 ± 430	−13.4 ± 0.4	6.5 ± 0.6	ND
Bt-AChBP	Carbamylcholine	721 ± 283	−14.1 ± 0.5	5.7 ± 0.3	ND
Ls-AChBP	*d*-Tubocurarine	42 ± 3	−6.9 ± 0.6	−3.0 ± 0.4	ND
Bt-AChBP	*d*-Tubocurarine[c]	20	−1.4	−8.9	ND
Ls-R104V	*d*-Tubocurarine	26 ± 5	−5.9 ± 0.1	−4.4 ± 0.2	ND
Ls-L112I	*d*-Tubocurarine	11 ± 4	−5.9 ± 0.1	−4.9 ± 0.2	ND
Ls-M114V	*d*-Tubocurarine	12 ± 4	−9.2 ± 0.3	−1.5 ± 0.6	ND
Ls-L112I/M114V	*d*-Tubocurarine	11 ± 3	−5.0 ± 0.5	−5.8 ± 0.4	ND
Ls-R104V/L112I/M114V	*d*-Tubocurarine	20 ± 2	−4.3 ± 0.2	−6.1 ± 0.1	ND

[a] Data were taken from Celie *et al.* (18).
[b] ND, not determined.
[c] Values for *d*-tubocurarine binding are an approximation, as explained under "Ligand Binding."

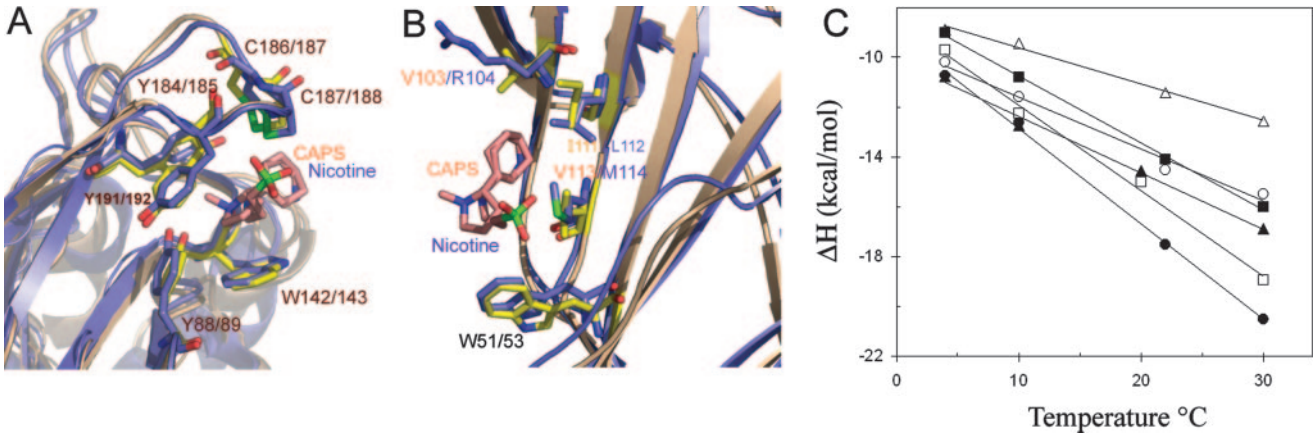

FIG. 7. **Substitution of binding site residues R104V, L112I, and M114V.** Opening-up of the AChBP ligand-binding site shows the principal (*A*) and complementary (*B*) binding site when Bt-AChBP (*yellow*, *wheat*) and Ls-AChBP (*blue*, *slate*) are superimposed. CAPS and nicotine molecules (*pink*, carbons) are shown; residue numbering is shown in *dark red* for Bt-AChBP/Ls-AChBP in the principal side (*A*) and *pink*/*blue* for Bt-AChBP/Ls-AChBP residues that have been exchanged in Ls-AChBP (*B*). *C*, titration of nicotine with Ls-AChBP (○), Bt-AChBP (●), Ls-AChBP-L112I (△), Ls-AChBP-M114V (▲), Ls-AChBP-R104V (■), Ls-AChBP-R104V/L112I/M114V (□) at 4, 10, 22, and 30 °C. ΔH is plotted against the temperature, and ΔC_p is obtained from the slope of the linear fittings.

The triple mutant Ls-AChBP R104V/L112I/M114V shows a clear gain-of-affinity for binding both nicotine and *d*-tubocurarine and mimics the affinities observed for the *Bulinus* protein. Because these mutations affect van der Waals contacts, we analyzed the effect of the substitutions on hydrophobic contact with the ligands using ITC. We measured ΔH of nicotine and acetylcholine binding to the various AChBPs at selective temperatures. ΔH is linearly dependent with temperature (Fig. 7*C*), and the slope of the line represents the change in heat capacity (ΔC_p). Because a negative ΔC_p value is an indication of the hydrophobic contribution to ligand binding (37), Bt-AChBP has more van der Waals contact to nicotine and acetylcholine than Ls-AChBP (Fig. 7*C*, Table II). The hydrophobic contribution to nicotine binding in the gain-of-affinity *Lymnaea* triple mutant AChBP has become equivalent to that in the Bt-AChBP. Thus, these three mutations contribute to make the Ls-AChBP -binding site resemble the Bt-AChBP. However, the remaining differences in entropic and enthalpic contribution as well as the acetylcholine binding effects show that regions outside the immediate binding site also contribute to the affinity.

DISCUSSION

In this study we cloned the AChBP gene from the snail *B. truncatus* and compared the structural and pharmacological properties of Bt-AChBP protein to that of Ls-AChBP. Bt-AChBP is expressed in glial cells of the central nervous system

of the animal (Fig. 1*D*). This is similar to the expression of Ls-AChBP, which is functionally implicated in the glial modulation of cholinergic synaptic transmission (7). Thus, we expect that the function of this protein is conserved. It is intriguing, however, that Bt-AChBP appears to be present as a stable "double pentamer" in solution in contrast to pentameric Ls-AChBP (8) and Ac-AChBP (19). Whether Bt-AChBP also behaves as a double pentamer *in vivo* remains to be established.

According to sequence identity, Bt-AChBP is more closely related to Ls-AChBP than Ac-AChBP (sequence identity between Bt-AChBP and Ls-AChBP is 41 *versus* 29% between Bt-AChBP and Ac-AChBP). This might be expected given the evolutionary distance between species (*Lymnaea versus Bulinus* estimated at 15 million years and *Lymnaea* (*Bulinus*) *versus Aplysia* at 600 million years).

It is interesting to compare the rate of evolution of the AChBPs with that of nicotinic receptor subunits in these species. The two known *Aplysia* nAChR subunits (accession numbers AAL37250 and AAL78648) share 47–86% sequence identity with nAChR subunits identified from *Lymnaea* central nervous system.[2] Thus, the AChBPs show significantly larger diversity (29%) than their receptor counterparts (>47%), indicating that the evolutionary pressure on conservation of the AChBP sequence is apparently less than for the nicotinic receptors.

Despite the diversity between Bt-AChBP, Ls-AChBP, and Ac-AChBP, all three AChBPs have maintained a similar level of sequence identity (11–28%) with the extracellular domains of all Cys-loop family members, indicating that the evolutionary pressure has preserved a minimal sequence scaffold between the entire LGIC family and AChBPs. Although the sequence conservation between Ls-AChBP and Bt-AChBP is low, the structure of Bt-AChBP is very similar to that of Ls-AChBP. This is an important validation for many modeling studies of various LGIC ligand binding domains that have used Ls-AChBP as a starting model. The comparison also reveals which regions are most variable in structure and provides alternative conformations for these variant regions. Residues of the subunit interface have not been conserved in Bt-AChBP and the other AChBPs as we noted before for the LGICs (8) except for the ligand binding residues. Apparently, the conserved ligand-binding site and the monomer interface form separate entities during evolution.

The changes in subunit interface contacts in Bt-AChBP and Ls-AChBP have an effect on protein stability (Fig. 5). This may also be the case for the nAChR ligand binding domains, because expression of these domains has proven remarkably difficult, and in many cases a mixture of monomers, dimers, and multimers was obtained (38, 39). Apparently the mode of pentamer formation is poorly conserved, and these extracellular domains may not have preserved the ability to form stable pentamers in the absence of their respective transmembrane regions. It will be useful to analyze the AChBP structures for regions that could improve the formation of stable pentamers in nicotinic structures.

The gain-of-affinity observed for nicotine binding to Ls/Bt-AChBP mutants indicates that residues 104, 112, and 114 (Ls-AChBP numbering) located in the ligand-binding site itself are mainly responsible for the difference in binding affinity. The contribution of these residues to ligand binding is compatible with altered binding capacities induced by mutagenesis of corresponding residues in nAChRs (40, 41). Our results for acetylcholine binding, however, imply that alternative residues outside the binding site also contribute to ligand binding. These may be part of the subunit interface but could also be located in other parts of the protein.

Binding of nAChR agonists to AChBP involves a large favorable enthalpy contribution that is counteracted by an unfavorable change in entropy. Binding of the nAChR antagonist *d*-tubocurarine in contrast is mediated by favorable changes in both enthalpy and entropy (Table II). The opposite effect of ΔS on agonist *versus* antagonist binding has also been reported for the nAChR receptor when ligand binding was analyzed at various temperatures using membrane homogenates that contain nAChRs (42, 43) and by measuring ligand-induced muscle contraction of denervated diaphragm (44, 45). A similar effect has been described for other members of the LGIC family and also for a number of G-protein-coupled receptors (43). Although this thermodynamic discrimination appears to be a common feature in ligand-receptor interaction, the mechanism underlying this phenomenon is not well understood. It does tell us, however, that the conformational changes upon ligand binding to AChBPs have the same character as binding to the nicotinic receptors, although the switch from enthalpy- to entropy-driven for agonist and antagonist binding is less dramatic compared with that of the LGICs.

Formation of the subunit interface is essential for the gating process in nAChR and other LGICs. Activation of the nAChR induced by agonist binding involves a switch in the relative orientation of subunits and induces channel opening (46). Although AChBP lacks a transmembrane region and seems to function as an acetylcholine buffer molecule rather than a signal transducer (7), recent experiments using Ls-AChBP/5-HT_{3A} chimeras have shown that AChBP can be functionally linked to a transmembrane domain (17). The fact that the AChBP protein is capable of changing conformation in a productive manner and providing the signal to open the receptor illustrates the significance of analyzing AChBP structures in addition to ligand binding capacities.

Because a high resolution structure of antagonist-bound AChBP is not available, we cannot compare conformational changes relative to our agonist-bound AChBP structures (18). However, one of the most striking differences between Ls- and Bt-AChBP is the conformation of a series of critical loops on the "bottom side" of the pentamer that would be close to the transmembrane region in the LGICs. Although other properties like crystallization conditions or variability in intrinsic protein structures could be responsible for these differences, it may also be possible that CAPS binding induces a change in these loops. The CAPS buffer molecule is larger than the nicotinic agonists that we have previously studied. Therefore, CAPS may resemble an antagonist in its binding mode, and it is possible that this pushes the structure into a state that approaches the "resting" state rather than the activated/desensitized state that was observed for the Ls-AChBP structures. Repositioning of the C-loop (residues 184–191, loop 10) upon CAPS binding could induce the observed rigid body movement of the loops 2, 7, and 11. This movement could be part of the conformational change that occurs upon transition of the resting state into the activated state (46). These loops would contact the transmembrane region in nAChRs and could, thus, stabilize the open state of the channel. This agrees well with a careful ϕ-value analysis (47) that these loops in nAChRs move as rigid bodies during gating (48). The comparison between resting and activated state by Unwin *et al.* (46) shows changes in electron density that have the same direction as we observe here. The changes that we observe, however, are much smaller and indicate that we probably do not yet see the complete

[2] P. van Nierop, S. Bertrand, D. Munno, Y. Gouwenberg, J. van Minnen, J. D. Spafford, N. I. Syed, D. Bertrand, and A. B. Smit, unpublished data.

features of the resting state. During the preparation of this manuscript, a 4.2-Å crystal structure of Ls-AChBP in complex with the nAChR-antagonist α-cobratoxin was reported (51). The structure shows conformational changes in C-loop and F-loop compared with our agonist-bound Ls-AChBP structures (18); however, no apparent changes were observed in loops 2, 7, and 11. The observation that these loops do not change conformation in the Ls-AChBP-α-cobratoxin structure is not understood yet but might be caused by the tight non-crystallographic symmetry that had to be maintained during refinement in addition to the relatively low resolution.

For the analysis of the structural conversion that is at the heart of the gating mechanism, it will be critical to have a good understanding of the conserved features of the structural LGIC scaffold to understand which regions are likely to be involved in the conserved opening of the ion channel. Thus, the Bt-AChBP structure presented here will provide critical help not only as an improved template for drug design based on these structures but also to understand how the LGIC gating is accomplished.

Acknowledgments—We thank Serge Cohen for assistance in using ARP/wARP, Roel van der Schors for mass spectrometry, Puck Knipscheer, Anastassis Perrakis, and the European Synchrotron Radiation Facility synchrotron staff for data collection, Bianca van Duyl for assistance in CD measurements, and Chris Ulens for critical reading of the manuscript.

REFERENCES

1. Ortells, M. O., and Lunt, G. G. (1995) *Trends Neurosci.* **18,** 121–127
2. Levin, E. D. (2002) *J. Neurobiol.* **53,** 633–640
3. Lindstrom, J. M. (2003) *Ann. N. Y. Acad. Sci.* **998,** 41–52
4. Laviolette, S. R., and van der Kooy, D. (2004) *Nat. Rev. Neurosci.* **5,** 55–65
5. Karlin, A. (2002) *Nat. Rev. Neurosci.* **3,** 102–114
6. Miyazawa, A., Fujiyoshi, Y., and Unwin, N. (2003) *Nature* **424,** 949–955
7. Smit, A. B., Syed, N. I., Schaap, D., van Minnen, J., Klumperman, J., Kits, K. S., Lodder, H., van der Schors, R. C., van Elk, R., Sorgedrager, B., Brejc, K., Sixma, T. K., and Geraerts, W. P. (2001) *Nature* **411,** 261–268
8. Brejc, K., van Dijk, W. J., Klaassen, R. V., Schuurmans, M., van Der Oost, J., Smit, A. B., and Sixma, T. K. (2001) *Nature* **411,** 269–276
9. Le Novere, N., Grutter, T., and Changeux, J. P. (2002) *Proc. Natl. Acad. Sci. U. S. A.* **99,** 3210–3215
10. Henchman, R. H., Wang, H. L., Sine, S. M., Taylor, P., and McCammon, J. A. (2003) *Biophys. J.* **85,** 3007–3018
11. Sullivan, D., Chiara, D. C., and Cohen, J. B. (2002) *Mol. Pharmacol.* **61,** 463–472
12. Schapira, M., Abagyan, R., and Totrov, M. (2002) *BMC Struct. Biol.* **2,** 1–8
13. Cromer, B. A., Morton, C. J., and Parker, M. W. (2002) *Trends Biochem. Sci.* **27,** 280–287
14. Trudell, J. (2002) *Biochim. Biophys. Acta* **1565,** 91–96
15. Laube, B., Maksay, G., Schemm, R., and Betz, H. (2002) *Trends Pharmacol. Sci.* **23,** 519–527
16. Reeves, D. C., and Lummis, S. C. (2002) *Mol. Memb. Biol.* **19,** 11–26
17. Bouzat, C., Gumilar, F., Spitzmaul, G., Wang, H. L., Rayes, D., Hansen, S. B., Taylor, P., and Sine, S. M. (2004) *Nature* **430,** 896–900
18. Celie, P. H., van Rossum-Fikkert, S. E., van Dijk, W. J., Brejc, K., Smit, A. B., and Sixma, T. K. (2004) *Neuron* **41,** 907–914
19. Hansen, S. B., Talley, T. T., Radic, Z., and Taylor, P. (2004) *J. Biol. Chem.* **279,** 24197–24202
20. Spijker, S., Smit, A. B., Eipper, B. A., Malik, A., Mains, R. E., and Geraerts, W. P. (1999) *FASEB J.* **13,** 735–748
21. Goldberg, F., Grunewald, B., Rosenboom, H., and Menzel, R. (1999) *J. Physiol.* (*Lond.*) **514,** 759–768
22. CCP4 (1994) *Acta Crystallogr. Sect. D* **50,** 760–763
23. Otwinowski, Z., and Minor, W. (1997) *Methods Enzymol.* **276,** 307–326
24. Perrakis, A., Morris, R., and Lamzin, V. S. (1999) *Nat. Struct. Biol.* **6,** 458–463
25. Jones, T. A., Zou, J. Y., Cowan, S. W., and Kjeldgaard, M. (1991) *Acta Crystallogr. A* **47,** 110–119
26. Winn, M. D., Isupov, M. N., and Murshudov, G. N. (2001) *Acta Crystallogr. D Biol. Crystallogr.* **57,** 122–133
27. Kleywegt, G. J., and Jones, T. A. (1997) *Methods Enzymol.* **277,** 525–545
28. Brunger, A. T., Adams, P. D., Clore, G. M., DeLano, W. L., Gros, P., Grosse-Kunstleve, R. W., Jiang, J. S., Kuszewski, J., Nilges, M., Pannu, N. S., Read, R. J., Rice, L. M., Simonson, T., and Warren, G. L. (1998) *Acta Crystallogr. D Biol. Crystallogr.* **54,** 905–921
29. Gouet, P., Courcelle, E., Stuart, D. I., and Metoz, F. (1999) *Bioinformatics* **15,** 305–308
30. West, A. P., Jr., Bjorkman, P. J., Dougherty, D. A., and Lester, H. A. (1997) *J. Biol. Chem.* **272,** 25468–25473
31. Vallee, B., Teyssier, C., Maget-Dana, R., Ramstein, J., Bureaud, N., and Schoentgen, F. (1999) *Eur. J. Biochem.* **266,** 40–52
32. Levandoski, M. M., Lin, Y., Moise, L., McLaughlin, J. T., Cooper, E., and Hawrot, E. (1999) *J. Biol. Chem.* **274,** 26113–26119
33. Zeng, H., Moise, L., Grant, M. A., and Hawrot, E. (2001) *J. Biol. Chem.* **276,** 22930–22940
34. Harel, M., Kasher, R., Nicolas, A., Guss, J. M., Balass, M., Fridkin, M., Smit, A. B., Brejc, K., Sixma, T. K., Katchalski-Katzir, E., Sussman, J. L., and Fuchs, S. (2001) *Neuron* **32,** 265–275
35. Balass, M., Katchalski-Katzir, E., and Fuchs, S. (1997) *Proc. Natl. Acad. Sci. U. S. A.* **94,** 6054–6058
36. Gao, F., Bern, N., Little, A., Wang, H. L., Hansen, S. B., Talley, T. T., Taylor, P., and Sine, S. M. (2003) *J. Biol. Chem.* **278,** 23020–23026
37. Sturtevant, J. M. (1977) *Proc. Natl. Acad. Sci. U. S. A.* **74,** 2236–2240
38. Schrattenholz, A., Pfeiffer, S., Pejovic, V., Rudolph, R., Godovac-Zimmermann, J., and Maelicke, A. (1998) *J. Biol. Chem.* **273,** 32393–32399
39. Tierney, M. L., and Unwin, N. (2000) *J. Mol. Biol.* **303,** 185–196
40. Sine, S. M. (1993) *Proc. Natl. Acad. Sci. U. S. A.* **90,** 9436–9440
41. Sine, S. M. (1997) *J. Biol. Chem.* **272,** 23521–23527
42. Borea, P. A., Varani, K., Gessi, S., Gilli, P., and Gilli, G. (1998) *Biochem. Pharmacol.* **55,** 1189–1197
43. Borea, P. A., Varani, K., Gessi, S., Merighi, S., Dal Piaz, A., Gilli, P., and Gilli, G. (2004) *Curr. Top. Med. Chem.* **4,** 361–368
44. Banerjee, B., and Ganguly, D. K. (1995) *Biochem. Pharmacol.* **49,** 1713–1716
45. Banerjee, B., and Ganguly, D. K. (1996) *Eur. J. Pharmacol.* **310,** 13–17
46. Unwin, N., Miyazawa, A., Li, J., and Fujiyoshi, Y. (2002) *J. Mol. Biol.* **319,** 1165–1176
47. Grosman, C., Zhou, M., and Auerbach, A. (2000) *Nature* **403,** 773–776
48. Chakrapani, S., Bailey, T. D., and Auerbach, A. (2004) *J. Gen. Physiol.* **123,** 341–356
49. Felsenstein, J. (1989) *Cladistics* **5,** 164–166
50. Wallace, A. C., Laskowski, R. A., and Thornton, J. M. (1995) *Protein Eng.* **8,** 127–134
51. Bourne, Y., Talley, T. T., Hansen, S. B., Taylor, P., and Pascale, M. (2005) *EMBO J.* **24,** 1512–1522